Pergamon

0301-9322(94)E0001-Y

Int. J. Multiphase Flow Vol. 20, No. 3, pp. 631–650, 1994

0301-9322/94 $7.00 + 0.00

INFLUENCE OF SHEAR-INDUCED MIGRATION ON TURBULENT RESUSPENSION

I. RAMPALL and D. T. LEIGHTON JR

Department of Chemical Engineering, University of Notre Dame, Notre Dame, IN 46556, U.S.A.

(Received 4 February 1992; in revised form 28 December 1993)

Abstract—In this paper we propose a model which predicts the point at which particles are first ejected from the viscous sublayer of a fluid flowing over a settled layer of particles into the turbulent core. The model, which combines viscous resuspension observations and an understanding of the structure of near-wall turbulence, is expected to be valid only for fine particles where the particle Reynolds number (based on the particle diameter and friction velocity) at resuspension is small. If a settled bed with fluid on top is sheared in a plane Couette device with the bottom plate fixed at low Reynolds nunber (based on the velocity of the top plate and the width of the gap), it has been shown that the shear-induced effective particle diffusivity arising from particle interactions causes the bed to expand. This expansion occurs in a narrow transition region between the settled bed and a region devoid of particles. If this region is thin with respect to the dimensions of the viscous sublayer of the flow, then the turbulent shear stress variations in the near-wall region will be impressed on the resuspending layer. Turbulent resuspension would be expected to occur by this mechanism when the bed has expanded enough that the upward velocity at some point in the resuspending layer caused by the turbulent eddies is greater than the downward settling due to gravity. By formulating the problem in this manner, the contribution of viscous effects to the onset of turbulent resuspension may be predicted from known quantities.

The dimensionless steady-state concentration profile caused by the interaction between viscous resuspension and turbulent eddies is found to be characterized by the parameter $S = \beta^+[(9/2)\psi]^2(9/2\psi)^2(\mathrm{Re}_p^+)$; where β^+ is the dimensionless magnitude of the vertical velocity of the eddies, measured previously to be $\beta^+ = 0.005$; ψ is the Shields parameter $\tau/\Delta\rho ga$, where τ is the wall shear stress, $\Delta\rho$ is the density difference between the particles and the fluid, g is the gravitational acceleration and a is the particle radius; and Re_p^+ is the particle Reynolds number $u*d_p/\nu$, where $u* = (\tau/\rho)^{1/2}$ is the friction velocity, d_p is the particle diameter, ν is the kinematic viscosity and ρ is the fluid density. The point at which the model predicts incipient turbulent resuspension to occur is given by $S \approx 5$. This point is shown to lie between the Shields criterion for the onset of first motion in a settled layer and the minimum flow condition for complete resuspension of a settled layer, suggesting that viscous effects do play an important role in incipient turbulent resuspension at low particle Reynolds numbers.

Key words: resuspension, bed erosion, sediment transport, shear-induced migration, mass transfer

1. INTRODUCTION

The resuspension and transport of sediments through pipelines and flumes is a fundamental problem in engineering. Perhaps the simplest example of sediment transport is the gravity-driven transport of a sedimenting slurry through an open channel, as depicted in figure 1. In this problem particles are convected along the channel by the fluid flow and, since they are negatively buoyant, tend to settle out. At steady state this sedimentation is balanced by some dispersive mechanism which acts to keep the particles in suspension. The balance between sedimentation and dispersion results in a concentration distribution which, in concert with the fluid velocity profile, determines the rate of sediment transport.

In order to predict this rate it is necessary to model the dispersive process which keeps the particles in suspension. The simplest model for this dispersion in the Prandtl mixing-length model, in which the particle dispersion is assumed to be the result of turbulent eddies carrying the particles across time-averaged streamlines. If we confine our attention to the region of the flow in which the shear stress is approximately constant (e.g. far from the upper free surface) and make the conventional assumption that the length scale of the mixing is proportional to the distance from the wall of the channel, then the dispersion coefficient is given by

$$D^t = (\kappa_s y)^2 \left| \frac{d\bar{v}_x}{dy} \right|, \qquad [1]$$

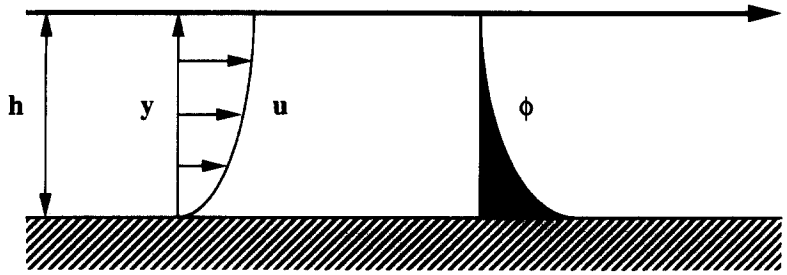

Figure 1. Concentration profile in the turbulent core of the flow obtained from a balance of the Stokes sedimentation flux and the dispersion due to Prandtl mixing.

where D^t is the turbulent density eddy diffusivity, κ_s is the Prandtl mixing-length constant, y is the distance from the wall and $\bar{v}_x$ is the time-averaged velocity. Again following the mixing-length arguments for momentum transport, the velocity gradient in the turbulent core is given by

$$\left|\frac{d\bar{v}_x}{dy}\right| = u_* \frac{1}{\kappa_s y}, \qquad [2]$$

where $u_* = (\tau_0/\rho)^{1/2}$ is the friction velocity, τ_0 is the wall shear stress and ρ is the fluid density.

At steady state in the turbulent core of the flow, we have a balance between this dispersive flux and the sedimentation flux:

$$N_y = -u_s f\phi - u_* \kappa_s y \frac{d\phi}{dy} = 0, \qquad [3]$$

where u_s is the Stokes settling velocity, f is the hindered settling factor and ϕ is the concentration. For dilute systems the hindered settling factor is unity, thus [3] may be integrated to obtain the well-known power-law concentration profile (Yalin 1972):

$$\phi = \phi_0 \left(\frac{y}{y_0}\right)^{-u_s/\kappa_s u_*}. \qquad [4]$$

Considering the simplicity of the model for particle dispersion, [4] describes the experimentally observed concentration profile in the turbulent core surprisingly well, as may be seen from figure 2.

A significant drawback to this model is that there is no way to predict the entire concentration profile *a priori* from the boundary conditions at the wall. This difficulty arises because the "mixing length", and hence the particle dispersion coefficient, vanishes at the wall. As a consequence, the concentration profile given in [4] must be fixed at some value ϕ_0 at an arbitrarily chosen "reference level" y_0—the so-called reference level problem (McTigue 1983). This difficulty is not at all surprising, since the physics of particle transport in the viscous sublayer of the flow differ from that governing transport in the turbulent core. For the case of the diffusion of *molecules* away from the wall there is little difficulty, since at some distance from the wall molecular diffusion becomes comparable to convective transport. Whether the convection is described by the simple model above, or by a more sophisticated model which includes the structure of near-wall turbulence, such as that developed by Campbell & Hanratty (1983), the balance between convection and diffusion provides a bridge from the diffusive viscous sublayer at the wall and the convection in the turbulent core. For particulate flows, however, molecular diffusion is negligible and some other mechanism must be found to disperse particles in the viscous sublayer.

Mechanisms which have been proposed for this dispersion include inertial lift, in which the inertia of the fluid flowing over the particles attached to the surface exerts an inertial lift balancing the sedimentation due to gravity, and turbulent microbursts, which penetrate to the wall to within 1 particle diameter (Thomas 1961). The reference level problem can be avoided entirely using a Lagrangian description for the case of large Stokes number flows, in which the inertia of the particles carries them entirely through the viscous sublayer. While these mechanisms will dominate resuspension processes at moderate and high particle Reynolds numbers Re_p^+ (a Reynolds number

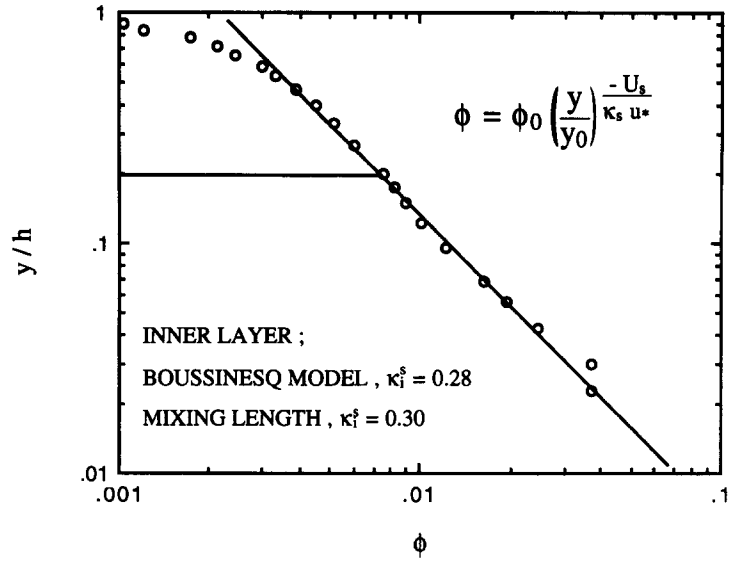

Figure 2. Comparison of the predicted power-law concentration profile (Yalin 1972) and measured concentrations in an open channel flow. [From McTigue (1983).]

based on the friction velocity and the particle diameter), they are unlikely to be significant at lower Reynolds numbers. Indeed, Yung *et al.* (1989) recently showed that turbulent microbursts were unable to entrain particles into the mean flow over the experimentally studied range $0.5 < Re_p^+ < 1.3$. Here we propose a new mechanism by which the ejection of particles from the viscous sublayer is predicted to occur under conditions when the particle Reynolds number is small and inertial effects are negligible.

When a settled bed of particles is sheared by turbulent flow of fluid, the surface of the bed is subjected to a mean stress due to the time-averaged bulk flow as well as spatially and temporally fluctuating wall shear stresses (Finnicum & Hanratty 1985). The magnitude of the fluctuating components is small compared to the mean wall shear stress. The first motion of the settled bed occurs when the Shields parameter (based on the mean shear stress) is greater than some critical value. The dependence of this critical Shields parameter on the Reynolds number of the flow (based on friction velocity and particle diameter) is referred to as the Shields diagram (Mantz 1977; Yalin & Karahan 1979). The first motion of the settled bed is characterized by a rolling or tumbling motion of particles on the surface of the bed.

At much higher values of the Shields parameter, the settled bed is found to resuspend even under viscous conditions (Gadala-Maria 1979; Leighton & Acrivos 1986). Thus, even if the particle Reynolds number is small, the mean shear stress causes the bed to expand in the viscous sublayer of the flow. If this bed expansion is combined with the convective motion induced by the spatial fluctuations of the shear stresses imposed on the viscous sublayer, then it is possible that the upward vertical velocity in some region within the resuspended layer may exceed the downward settling due to gravity, thus causing an ejection of the particles into the turbulent core of the flow. In this paper we propose this new mechanism for turbulent resuspension, which involves the viscous mechanism of shear-induced migration.

The model presented here is intended solely to determine the conditions under which the viscous mechanism of shear-induced migration significantly influences the turbulent resuspension process. As a consequence of the limitations of the model, we are not attempting to predict the point at which the first sediment motion occurs, or the actual sediment transport rate. Rather, we predict the point at which particles are first ejected from the viscous sublayer into the turbulent core of the flow. This should correspond to an abrupt increase in the rate of sediment transport as particles are entrained in high-velocity regions.

In the next section we briefly describe the shear-induced migration process, which has been identified to result in the resuspension of a settled layer of particles under purely viscous flow

conditions. In section 3 we combine this shear-induced migration mechanism with a simple model of near-wall turbulence and derive the general mass-balance equation which models the resuspension phenomenon in the viscous sublayer at low Reynolds number. In section 4 we solve a linear approximation to this model, which provides us with insight into the behavior of the resuspending layer and which is useful in its own right for the corresponding problem of the mass transfer of molecular species in the presence of an externally applied force field. In section 5 we develop and solve the full nonlinear convection–diffusion model of a resuspended particle layer with moving boundaries. In the final section, we will compare the predictions made by this new model with previous experimental results and with inertial lift mechanisms.

2. VISCOUS RESUSPENSION

Gadala-Maria (1979) observed that when a coal oil slurry in a parallel-plate viscometer was sheared after being allowed to rest overnight, the torque signal initially measured by the viscometer was quite small. Over a short period of time, however, it increased to the steady-state values observed the previous day. He was able to quantitatively account for this increase in the torque signal by the resuspension of coal particles which, during the period of rest, had formed a settled layer. This resuspension process was not associated with turbulence, since the Reynolds number based on the gap width was on the order of 10^{-2} or smaller.

The phenomenon was investigated more completely by Leighton & Acrivos (1986, 1987), who demonstrated that the viscous resuspension of the settled particles could be accounted for by an effective diffusivity which was proportional to the shear rate and the square of the particle radius. Because of the observed dimensional scaling, the effective diffusivity was attributed to the interactions which occurred between particles as a suspension was sheared, and thus the term shear-induced effective diffusion was used to describe the phenomenon. The magnitude of the shear-induced effective diffusivity was measured in a distinct experimental geometry to be a strong function of concentration which vanished as the concentration approached zero (Leighton & Acrivos 1987). The effective diffusivity for suspensions of several types of particles has subsequently been measured with greater accuracy by Chapman & Leighton (1991), who found that while the diffusivity varied between suspensions at the same concentration in much the same manner as the suspension viscosity, the correlation proposed by Leighton & Acrivos (1986) provided a reasonable description of the data:

$$D = \dot{\gamma} a^2 / \hat{D}, \qquad [5]$$

where $\hat{D}$ is given by

$$\hat{D} = \tfrac{1}{3}\phi^2(1 + \tfrac{1}{2}\mathrm{e}^{8.8\phi}). \qquad [6]$$

A plot of the effective diffusivity as a function of concentration is given in figure 3.

3. NEAR-WALL TURBULENCE

The viscous resuspension phenomenon described above immediately suggests a possible way by which incipient *turbulent* resuspension at low particle Reynolds numbers may occur. Even though the Reynolds number of a flow may be large based on the length scale of a pipe or channel, in the vicinity of the wall the particle Reynolds number ($\mathrm{Re}_\mathrm{p}^+ = u_* \rho d_\mathrm{p}/\mu$, where d_p is the particle diameter and μ is the viscosity) may be quite small. Under such circumstances it seems reasonable that, due to the large applied shear stresses in the near-wall region of a turbulent flow, the interaction between particles in this shear flow should give rise to the same type of viscous shear-induced effective diffusivity as was observed in the viscous resuspension experiments. This suggests that in the vicinity of the wall the shear stress and the resulting shear-induced migration

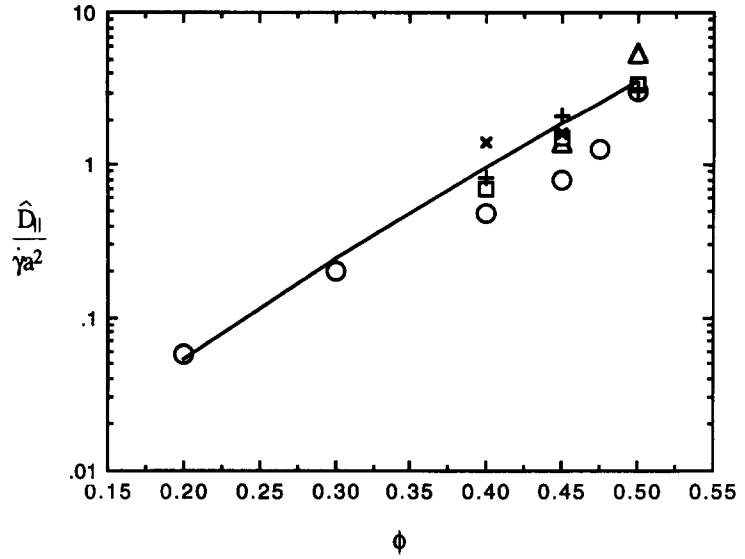

Figure 3. Plot of the measured effective shear-induced diffusivity in concentrated suspensions by Leighton & Acrivos (1985) (+, ×, −) and Chapman & Leighton (1991) (○, △, □): ○, 115 μm glass spheres; △, 46 μm polystyrene spheres; □, 47 μm glass spheres; +, 46 μm polystyrene spheres; ×, 86 μm polystyrene spheres; ——, diffusivity correlation.

due to the interaction between particles would cause a settled bed of particles to expand. This expansion would then permit particles to escape the viscous sublayer and be swept out by the turbulent eddies into the turbulent core.

In order to develop the qualitative idea described above into a quantitative model of turbulent resuspension, we must first examine the detailed structure of the turbulence in the viscous sublayer. For the purposes of our model, we shall assume that the structure of the near-wall turbulence over a settled bed is the same as that over a smooth wall. This is likely to be true only if the particle diameter is small relative to the viscous length scale $\nu/(\tau/\rho)^{1/2}$, where ν is the kinematic viscosity. This is equivalent to requiring that the particle Reynolds number based on the friction velocity be small. For uniform flow over a plane, Finnicum & Hanratty (1985) demonstrated that the dominant features of the turbulence in the viscous sublayer leading to vertical convective mass transfer are counter-rotating eddies with vorticity axes aligned with the main flow.

We apply this picture of near-wall turbulence to our viscous resuspension model with the assumption that the turbulent shear stress, which gives rise to these counter-rotating eddies, is impressed on the resuspending particle layer. The influence of the particles on the turbulent stresses is ignored since, as shall be demonstrated, the thickness of the resuspending layer is very thin with respect to the size of the turbulent eddies. The stresses are thus imposed on this resuspending layer in the same manner as on any mass transfer boundary layer.

The turbulent shear stresses are a perturbation on the time-averaged wall shear stress $\tau_0 = \langle \tau_{yz} \rangle$ as follows:

$$\tau_{yz}(x, z, t) = \tau_0 + \tau'_{yz}(x, z, t) \qquad [7]$$

and

$$\tau_{yx}(x, z, t) = \tau'_{yz}(x, z, t). \qquad [8]$$

The flow geometry is depicted in figure 4. The shear stresses τ_{yz} and τ_{yx} in [7] and [8] are obtained as the first term of a Taylor series expansion with respect to the distance y from the wall and hence are valid in the limit as $y \to 0$.

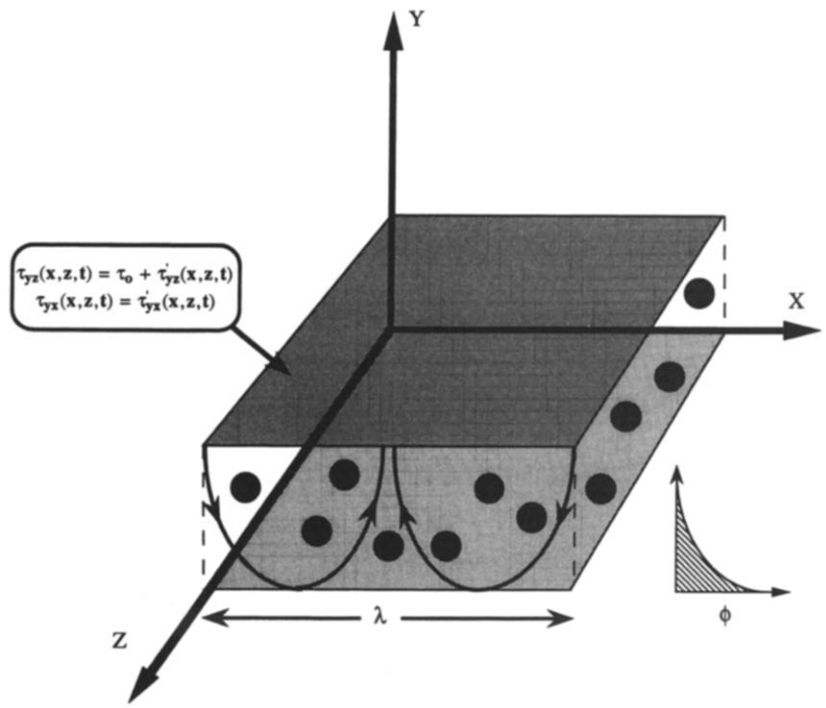

Figure 4. Counter-rotating eddy structure in the near-wall region due to fluctuating turbulent shear stresses imposed on the viscous sublayer.

The flow field in the resuspended layer is obtained by solving the shear stress and continuity equations in a thin resuspended layer of particles near the fully packed layer:

$$\tau_{yz} = \mu \frac{\partial u_z}{\partial y}, \qquad [9]$$

$$\tau_{yx} = \mu \frac{\partial u_x}{\partial y} \qquad [10]$$

and

$$\frac{\partial u_x}{\partial x} + \frac{\partial u_y}{\partial y} + \frac{\partial u_z}{\partial z} = 0, \qquad [11]$$

where μ will be a function of the concentration distribution and hence of both position and time. Equations [9]–[11] can be rewritten in terms of the relative viscosity $\mu_r = \mu/\mu_0$ (where μ_0 is the viscosity of the suspending fluid) and integrated to yield equations for the velocity field in the resuspended layer:

$$u_x = \frac{\tau'_x(x, z, t)}{\mu_0} \int_{-\infty}^{y} \frac{1}{\mu_r(x, y, z, t)} \mathrm{d}y, \qquad [12]$$

$$u_z = \frac{(\tau_0 + \tau'_z(x, z, t))}{\mu_0} \int_{-\infty}^{y} \frac{1}{\mu_r(x, y, z, t)} \mathrm{d}y \qquad [13]$$

and

$$u_y = -\int_{-\infty}^{y} \left(\frac{\partial u_x}{\partial x} + \frac{\partial u_z}{\partial z} \right) \mathrm{d}y. \qquad [14]$$

Since the relative viscosity of a fully settled layer is infinite, only those regions over which the concentration is less than that at maximum packing will contribute to the velocity field. In the case of a settled bed with clear fluid above (i.e. $\mu_r = 1$), the equations can be solved for the flow field

in the vicinity of a wall in terms of the shear rates $s_x = \tau'_{yx}/\mu_0$ and $s_z = \tau'_{yz}/\mu_0$ and $S_z = \tau_0/\mu_0$ along the x- and z-directions as follows:

$$u_x = s_x(x, z, t)y, \quad [15]$$

$$u_z = (S_z + s_z(x, z, t))y \quad [16]$$

and

$$u_y = \beta y^2, \quad [17]$$

where β is given by

$$\beta(x, z, t) = -\frac{1}{2}\left(\frac{\partial s_x}{\partial x} + \frac{\partial s_z}{\partial z}\right). \quad [18]$$

Finnicum & Hanratty (1985) have measured the vertical velocity fluctuations in the vicinity of the wall and have reported a mean square value $\beta^+ = \nu^2\langle\beta^2\rangle^{1/2}/u_*^3 = 0.005$ for the dominant eddies. The vertical velocity due to fluctuating shear stress in the z-direction has been shown to contribute only 5% to the measured value of β, which agrees with the scaling arguments of Campbell & Hanratty (1983). Hence, the dominant contribution to the vertical motion is a result of turbulent fluctuations transverse to the main time-averaged flow in the z-direction. We therefore approximate the three-dimensional turbulent flow by a two-dimensional velocity field (u_x, u_y) and neglect any variation in the direction of the main flow. This geometry is depicted in figure 4. Following Finnicum & Hanratty (1985), we assume the counter-rotating turbulent eddies transverse to the direction of flow to be characterized by a width λ and an amplitude α:

$$s_x = \alpha(t)\sin\frac{2\pi x}{\lambda}. \quad [19]$$

From the continuity equation [18], α, β and λ are related to each other by

$$\beta = \frac{1}{2}\left(\frac{2\pi\alpha}{\lambda}\right). \quad [20]$$

The flow field due to the counter-rotating eddies for the case of a resuspended layer of particles is formulated in terms of the velocity components u and v in the x- and y-directions, respectively:

$$u = \alpha \sin\frac{2\pi x}{\lambda}\int_{-\infty}^{y}\frac{1}{\mu_r}\,dy' \quad [21]$$

$$\frac{\partial u}{\partial x} = \frac{2\pi\alpha}{\lambda}\cos\frac{2\pi x}{\lambda}\int_{-\infty}^{y}\frac{1}{\mu_r}\,dy' - \alpha\sin\frac{2\pi x}{\lambda}\int_{-\infty}^{y}\frac{1}{\mu_r^2}\frac{d\mu_r}{d\phi}\frac{\partial\phi}{\partial x}\,dy' \quad [22]$$

and

$$v = -\frac{2\pi\alpha}{\lambda}\cos\frac{2\pi x}{\lambda}\int_{-\infty}^{y}\int_{-\infty}^{y'}\frac{1}{\mu_r}\,dy''\,dy' + \alpha\sin\frac{2\pi x}{\lambda}\int_{-\infty}^{y}\int_{-\infty}^{y'}\frac{1}{\mu_r^2}\frac{d\mu_r}{d\phi}\frac{\partial\phi}{\partial x}\,dy''\,dy'. \quad [23]$$

Combining the convective flux, arising as a result of the eddy motion, with the transport fluxes, due to sedimentation and shear-induced diffusion, we obtain the equations for total particle flux in the x- and y-directions:

$$N_x = u\phi \quad [24]$$

and

$$N_y = v\phi - D\frac{\partial\phi}{\partial y} - u_s f\phi, \quad [25]$$

where u_s is the Stokes settling velocity in an unbounded stagnant fluid, f is the hindered settling factor and D is the concentration-dependent shear-induced diffusion coefficient. Hunt (1954) has suggested that the sedimentation velocity be modified by the induced upward velocity of the suspending fluid due to the downward motion of the particles. While this correction is likely to

become important in highly concentrated polydisperse suspensions as $\phi \to 1$, it is always bounded by the finite maximum packing fraction for the monodisperse suspensions considered here. In any event, this effect can be absorbed into the hindered settling function f.

The flux relations can be used to obtain the transient mass-conservation equations for the particles in the resuspended layer:

$$\frac{\partial \phi}{\partial t} = -\nabla \cdot \mathbf{N}$$

$$= -u\frac{\partial \phi}{\partial x} - v\frac{\partial \phi}{\partial y} + \frac{\partial}{\partial y}\left(D\frac{\partial \phi}{\partial y}\right) + \frac{\partial}{\partial y}(u_s f \phi), \qquad [26]$$

where we have neglected diffusion in the x-direction relative to convection and all variations in the z-direction.

4. MASS TRANSFER IN SEDIMENTING SYSTEMS

While [26] could, in principle, be solved numerically for the time-dependent evolution of the concentration profile, it is instructive to first consider a simpler limiting form. We shall examine the case when the diffusion coefficient D is constant, the hindered settling factor f is unity and the boundaries do not move as a result of erosion/deposition of particles at the wall. Further, let us assume that sufficient time has elapsed for the concentration profiles to reach a steady state. The resulting problem is thus that of mass transfer of a sedimenting species undergoing molecular diffusion in the limit when the concentration is infinitely dilute. The steady-state mass-balance equation reduces to the simple convection–diffusion problem:

$$\alpha y \sin\frac{2\pi x}{\lambda}\frac{\partial \phi}{\partial x} = \frac{\pi \alpha}{\lambda} y^2 \cos\frac{2\pi x}{\lambda}\frac{\partial \phi}{\partial y} + D\frac{\partial^2 \phi}{\partial y^2} + u_s\frac{\partial \phi}{\partial y}. \qquad [27]$$

We impose the boundary conditions for $\phi = \phi_0$ at the wall $y = 0$ and $\phi \to \phi_\infty$ as $y \to \infty$. Because we have neglected diffusion in the x-direction, [27] involves only first-order derivatives in x. We thus must provide an initial condition in the downwelling region $x = 0$. This initial condition is obtained by substituting $x = 0$ in [27] and solving the resulting equation (now solely a function of y) for the initial concentration profile. As we shall demonstrate presently, the concentration distribution is independent of x for $x/\lambda \ll 1$, in the same manner as mass transfer is in stagnation flow.

It is useful at this point to render the equations dimensionless. We define $\phi^* = (\phi - \phi_\infty)/(\phi_0 - \phi_\infty)$ and $x^* = x/(\lambda/2\pi)$, so that the dimensionless width of a single eddy (one half of the pair) is equal to π. The scaling for y involves a choice among two length scales. The first length scale $L_c = (D/2\beta)^{1/3}$ is obtained by balancing the diffusion and vertical convection terms in [27], while the second length scale $L_s = D/u_s$ is obtained by balancing the diffusion and sedimentation terms. We choose the latter scaling, thus $y^* = y/L_s = yu_s/D$ and

$$Sy^* \sin x^* \frac{\partial \phi^*}{\partial x^*} = \left(S\frac{y^{*2}}{2}\cos x^* + 1\right)\frac{\partial \phi^*}{\partial y^*} + \frac{\partial^2 \phi^*}{\partial y^{*2}}. \qquad [28]$$

Note that the dimensionless differential equation is a function of the single dimensionless parameter $S = (L_s/L_c)^3$, which is the ratio of convection to sedimentation. The boundary conditions for the concentration are transformed to $\phi^* = 1$ at the wall $y^* = 0$ and $\phi^* \to 0$ as $y^* \to \infty$. The quantity of primary interest is the average mass transfer rate $\langle N_y \rangle$ from the wall. This is defined in terms of the concentration distribution by

$$\langle N_y \rangle = \frac{2}{\lambda}\int_0^{\lambda/2}\left(-D\frac{\partial \phi}{\partial y} - \phi_0 u_s\right)dx. \qquad [29]$$

We render the mass flux $\langle N_y \rangle$ into dimensionless form by scaling it with the sedimentation flux $u_s(\phi_0 - \phi_\infty)$:

$$\langle N_y \rangle^* = \frac{\langle N_y \rangle}{u_s(\phi_0 - \phi_\infty)} = \left(-\frac{1}{\pi} \int_0^\pi \frac{\partial \phi^*}{\partial y^*} dx^* - 1 \right) - \left[\frac{\dfrac{\phi_\infty}{\phi_0}}{1 - \dfrac{\phi_\infty}{\phi_0}} \right]. \quad [30]$$

In [30], for the dimensionless flux, we note that since the concentration profile ϕ^* is independent of ϕ_∞, we can represent $\langle N_y \rangle^*$ in terms of the first term in parentheses on the right-hand side of the equation, the value of which remains unchanged for all values of ϕ_∞, minus the second term which involves the parameter ϕ_∞/ϕ_0. We define a dimensionless flux $\langle N_{y_0} \rangle^*$ as equal to $\langle N_y \rangle^*$ when $\phi_\infty = 0$ and solve for the dimensionless flux for all values of ϕ_∞ in terms of $\langle N_{y_0} \rangle^*$ by

$$\langle N_y \rangle^* = \langle N_{y_0} \rangle^* - \frac{\dfrac{\phi_\infty}{\phi_0}}{1 - \dfrac{\phi_\infty}{\phi_0}}. \quad [31]$$

The dimensional flux from the wall can now be simply expressed as the upward flux due to diffusion [proportional to the driving force term $(\phi_0 - \phi_\infty)$] minus the flux of particles due to downward settling, which is impressed on the boundary layer from infinity:

$$\langle N_y \rangle = \langle N_{y_0} \rangle^* u_s(\phi_0 - \phi_\infty) - u_s \phi_\infty. \quad [32]$$

The concentration profile at $x^* = 0$ is obtained by substituting $x^* = 0$ in [28] and solving the linear ordinary differential equation for $\phi(0, y^*)$, to yield:

$$\phi(0, y^*) = \frac{\displaystyle\int_{y^*}^\infty \exp\left[-\left(S\frac{y^{*3}}{6} + y^* \right) \right] dy^*}{\displaystyle\int_0^\infty \exp\left[-\left(S\frac{y^{*3}}{6} + y^* \right) \right] dy^*}. \quad [33]$$

It is convenient to obtain the solution to [28] by making the substitution $\phi^*(x^*, y^*) = \phi^*(0, y^*) + \phi'(x^*, y^*)$, where ϕ' represents the deviation in the concentration distribution from the analytic result at $x^* = 0$. Equation [28] is transformed by this new choice of the dependent variable, to yield:

$$Sy^* \sin x^* \frac{\partial \phi'}{\partial x^*} = \left(S\frac{y^{*2}}{2} \cos x^* + 1 \right) \frac{\partial \phi'}{\partial y^*} + \frac{\partial^2 \phi'}{\partial y^{*2}} + (\cos x^* - 1) \frac{\partial \phi^*(0, y^*)}{\partial y^*}. \quad [34]$$

Equation [34] is an inhomogeneous equation due to a forcing term which arises from the known function $\phi(0, y^*)$, but with homogeneous boundary conditions $\phi' = 0$ at $y^* = 0$ and $y^* \to \infty$.

We note that the general solution to [34] is a sum of the solution to the homogeneous part of the equation and any particular solution to the problem. The homogeneous equation possesses a regular singular point at $x^* = 0$ and hence admits a solution which, in general, is not analytic at the origin. It is simple to demonstrate, however that [34] possesses a unique solution which is analytic at the origin, and for which $\partial \phi'/\partial x^* = 0$ at $x^* = 0$.

Equation [34] is solved numerically by integrating in the x^*-direction from $x^* = 0$ up to $x^* = \pi$. The Laplacian operator $\partial^2 \phi'/\partial y^{*2}$ is approximated by the three-point central-difference formula and the resulting set of coupled ordinary differential equations are integrated by the Crank–Nicholson implicit scheme to ensure stability. The boundary condition $\phi' = 0$ as $y^* \to \infty$ is implemented numerically, by solving a sequence of problems with $\phi' = 0$ at some chosen value $y^* = L_n$ until convergence in the integrated flux is obtained with increasing values of L_n. The integration of the concentration profile is performed up to $(\pi - \epsilon)$, where ϵ is typically 10^{-4}. This is required, since the convective velocity u is equal to zero at $x^* = \pi$ and hence $\partial \phi'(x^*, y^*)/\partial x^*$ is not defined at this point. The concentration profile $\phi(\pi, y^*)$ may be obtained analytically by

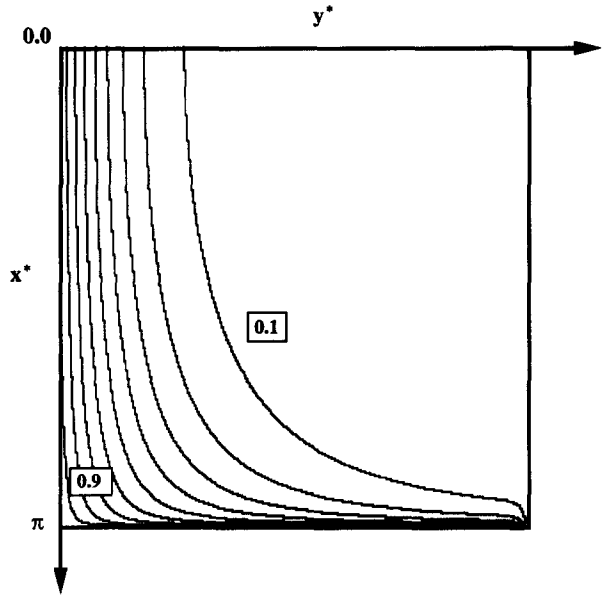

Figure 5. Plot of the concentration contours within the counter-rotating eddies from $\phi^* = 0.1$ up to $\phi^* = 0.9$. Note the concentration is nearly independent of x^* in the downflow region up to $x^* = \pi/2$. In the upflow region, the net mass flux far away from the wall is convected away from a narrow plume centered about $x^* = \pi$.

substituting $x^* = \pi$ in [28] and solving the resulting equation in y^*:

$$\phi^*(\pi, y^*) = \frac{\displaystyle\int_{y^*}^{L_n} \exp\left(S\frac{y^{*3}}{6} - y^*\right) dy^*}{\displaystyle\int_{0}^{L_n} \exp\left(S\frac{y^{*3}}{6} - y^*\right) dy^*}. \qquad [35]$$

It is interesting to examine the solution of [34] in the region $x^* = \pi - \epsilon$. From the analytic solution given in [35], we find that the dimensionless concentration at $x^* = \pi$ is unity everywhere except in a small region near $y^* = L_n$, where we have a sharp concentration gradient to match the imposed condition $\phi^* = 0$ at $y^* = L_n$. If we examine the total flux $\langle N_y \rangle^*$ across some plane which is well above the resuspending layer but well below $y^* = L_n$, we find that particles are ejected from the resuspending layer in a narrow plume centered about $x^* = \pi$. The width of this plume is a function of y^* and, from a mass balance, is given approximately by $2\pi\langle N_y \rangle^*/Sy^{*2}$. It is also interesting to note that the maximum rate of bed erosion occurs in the center of the downwelling region $x^* = 0$ and maximum deposition occurs at $x^* = \pi$. The concentration contour plot for various values of ϕ^* is depicted in figure 5.

The results of the numerical simulation are summarized in figure 6, where we plot the average flux $\langle N_y \rangle^*$ as a function of $S^{1/3}$ for various values of the parameter ϕ_∞/ϕ_0. The diffusive flux vanishes for small S, followed by a transition region. For large values of S, the dimensionless flux asymptotically approaches the line given by $\langle N_y \rangle^* = 0.46029S^{1/3} - \phi_\infty/\phi_0/(1 - \phi_\infty/\phi_0)$. This is the scaling expected for $\langle N_y \rangle^*$ if gravity plays no role in the erosion process.

5. TURBULENT RESUSPENSION

In order to solve the full resuspension model given by [26], we must obtain the constitutive equations for the effective diffusivity D, the hindered settling factor f and the relative viscosity μ_r as functions of the particle volume fraction ϕ. We shall assume the effective diffusivity to be given by [5] and the relative viscosity correlation reported by Leighton & Acrivos (1987) for suspensions

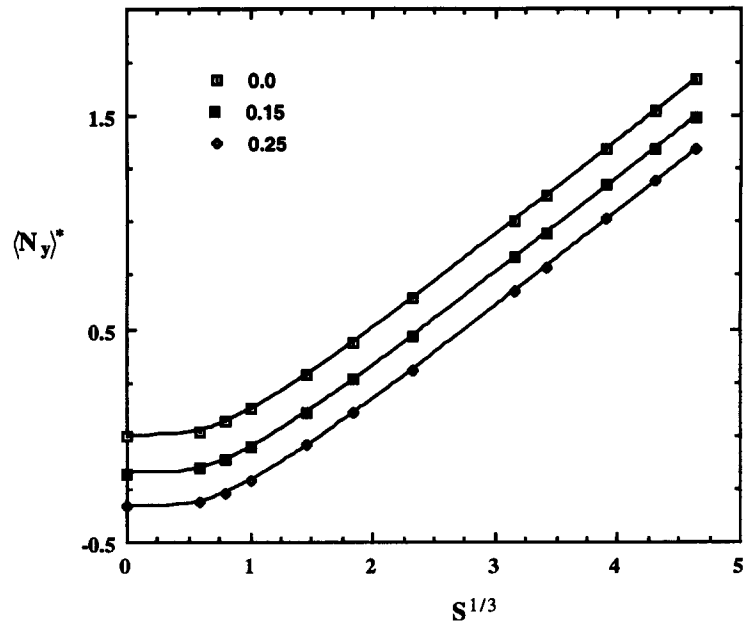

Figure 6. Plot of the dimensionless flux from the wall as a function of the dimensionless parameter $S^{1/3}$ for $\phi_\infty = 0$, 0.15, and 0.25 for the case of mass transfer in sedimenting systems.

of polystyrene spheres:

$$\frac{\mu}{\mu_0} = \left(1 + \frac{\frac{1}{2}[\eta]\phi}{1 - \frac{\phi}{\phi_m}}\right)^2, \qquad [36]$$

where $[\eta] = 3.0$ and $\phi_m = 0.58$. We shall also take the hindered settling factor f to be given by the Richardson–Zaki correlation:

$$f = (1 - \phi)^{5.1}. \qquad [37]$$

The convective velocity terms u and v, given by [21] and [23] respectively, are substituted in the mass-conservation equation [26]. The shear-induced diffusion coefficient D, given by [5], is rewritten by replacing the shear rate $\dot{\gamma}$ by $\tau_0/(\mu_0\mu_r)$. The resulting expression for D is substituted in [26] to obtain the nonlinear convection–diffusion model:

$$\frac{\partial\phi}{\partial t} = -\left(\alpha \sin\frac{2\pi x}{\lambda}\int_{-\infty}^{y}\frac{1}{\mu_r}\,dy'\right)\frac{\partial\phi}{\partial x} + \left(\frac{2\pi\alpha}{\lambda}\cos\frac{2\pi x}{\lambda}\right.$$
$$\left.\times\int_{-\infty}^{y}\int_{-\infty}^{y'}\frac{1}{\mu_r}\,dy''\,dy' - \alpha\sin\frac{2\pi x}{\lambda}\int_{-\infty}^{y}\int_{-\infty}^{y'}\frac{1}{\mu_r^2}\frac{d\mu_r}{d\phi}\,dy''\,dy'\right)\frac{\partial\phi}{\partial y}.$$
$$+\frac{\tau a^2}{\mu_0}\frac{\partial}{\partial y}\left(\frac{\hat{D}}{\mu_r}\frac{\partial\phi}{\partial y}\right) + u_s\frac{\partial(f\phi)}{\partial y}. \qquad [38]$$

Equation [38] is rendered dimensionless by defining $x^* = x/(\lambda/2\pi)$, $y^* = y/L_s$ and $t^* = t/t_0$, where L_s and t_0 remain to be determined. The characteristic length scale L_s in the y-direction is chosen to balance the shear-induced diffusion and sedimentation terms in [38] and hence becomes equal to $\tau a^2/u_s\mu_0$. This scaling for y is similar to the viscous resuspension length scale obtained by Leighton & Acrivos (1986) in the study of viscous resuspension. Substituting Stokes law for u_s we find $L_s = (9/2)\psi a$, where ψ is the Shields parameter (the ratio of viscous to buoyancy forces) $\tau/\Delta\rho g a$. We also note that since $\tau a^2/\mu_0$ is the dimensional scaling of the shear-induced diffusion coefficient, the length scale L_s is proportional to that used in the linearized problem examined in the previous section. The steady concentration profile will be attained over the time for particles

to diffuse over the length scale L_s, thus we choose $t_0 = L_s^2/[\tau a^2/\mu_0] = \tau a^2/\mu_0 \mu_s^2$. In dimensionless form, [38] thus becomes

$$\frac{\partial \phi}{\partial t^*} = -S\left(\sin x^* \int_{-\infty}^{y^*} \frac{1}{\mu_r}\, dy'\right)\frac{\partial \phi}{\partial x^*} + S\left(\cos x^* \int_{-\infty}^{y^*}\int_{-\infty}^{y'} \frac{1}{\mu_r}\, dy''\, dy' - \sin x^* \int_{-\infty}^{y^*}\int_{-\infty}^{y'} \frac{1}{\mu_r^2}\frac{d\mu_r}{d\phi}\frac{\partial \phi}{\partial x^*}\, dy''\, dy'\right)\frac{\partial \phi}{\partial y^*} + \frac{\partial}{\partial y^*}\left(\frac{\hat{D}}{\mu_r}\frac{\partial \phi}{\partial y^*}\right) + \frac{\partial (f\phi)}{\partial y^*}. \quad [39]$$

As in the linearized case, [39] depends upon a single parameter S defined here as $2\beta L_s^3 \mu_0/\tau_0 a^2$. We can represent the parameter S in terms of the particle Reynolds number by expressing L_s in terms of the Shields parameter ψ and β in terms of the dimensionless scaling for vertical motion β^+:

$$S = \beta^+\left(\frac{9}{2}\psi\right)^3 \mathrm{Re}_p^+. \quad [40]$$

Unlike the linearized problem, in which the lower boundary was assumed to be fixed at $y^* = 0$, in the nonlinear formulation the lower boundary will move as the bed erodes in the downwelling region and deposits in the upwelling region. In addition, there will be a sharp transition between the resuspending layer and the sedimenting suspension above it. In the special case of pure fluid above the resuspending layer, this transition will be a discontinuity in the slope of the concentration profile, because the diffusivity, which smooths out such discontinuities, vanishes as $\phi \to 0$. As a result, [39] is valid only within the resuspended layer of particles, where the concentrations are in the range given by $(0 < \phi < \phi_m)$ and additional equations must be developed to account for the moving boundaries.

We account for the movement of the boundaries by introducing the additional dimensionless variables $y_b^*(x^*, t^*)$ and $y_t^*(x^*, t^*)$, as shown in figure 7, which locate the position of the bottom and top boundaries as a function of time and position. These new variables are scaled with the

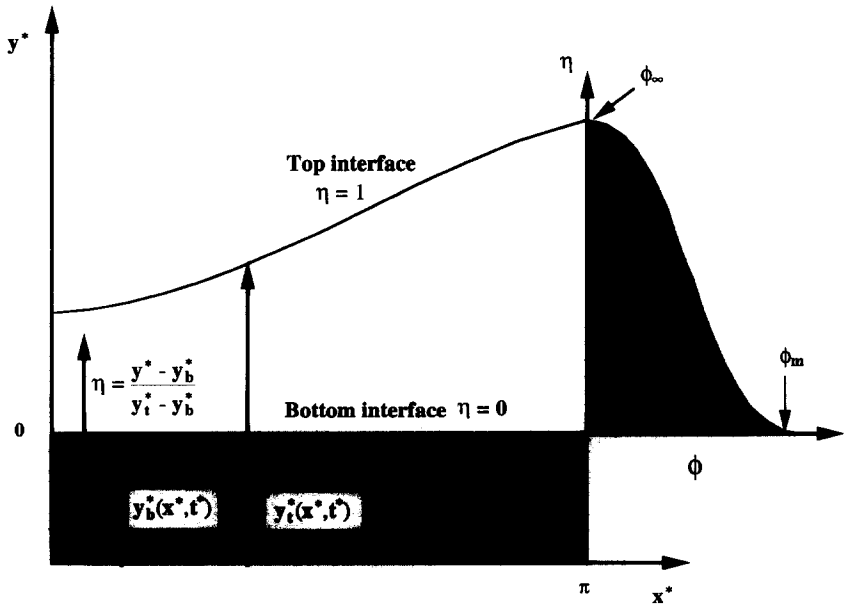

Figure 7. The resuspended layer of particles consists of a bottom settled layer which is essentially flat and a top interface. The y^* coordinate is transformed to $\eta = 0$ (the bottom settled layer of particles, where $\phi = \phi_m$) and $\eta = 1$ (the top edge of the resuspended layer, where $\phi = \phi_\infty$).

viscous resuspension length scale L_s. The y^* coordinate is transformed to another variable η, defined in terms of y_b^* and y_t^* as

$$\eta = \frac{y^* - y_b^*(x^*, t^*)}{y_t^*(x^*, t^*) - y_b^*(x^*, t^*)}. \qquad [41]$$

Hence, the bottom and top boundaries of the resuspended layer are mapped onto $\eta = 0$ and $\eta = 1$, respectively, and the partial derivative terms are transformed from the (x^*, y^*, t^*) coordinates to (x^*, η, t^*) coordinates:

$$\frac{\partial \phi(x^*, y^*, t^*)}{\partial x^*} = \frac{\partial \phi(x^*, \eta, t^*)}{\partial x^*} + \frac{\partial \phi(x^*, \eta, t^*)}{\partial \eta} \frac{\partial \eta(x^*, y^*, t^*)}{\partial x^*},$$

$$\frac{\partial \phi(x^*, y^*, t^*)}{\partial y^*} = \frac{\partial \phi(x^*, \eta, t^*)}{\partial \eta} \frac{\partial \eta(x^*, y^*, t^*)}{\partial y^*}$$

and

$$\frac{\partial \phi(x^*, y^*, t^*)}{\partial t^*} = \frac{\partial \phi(x^*, \eta, t^*)}{\partial t^*} + \frac{\partial \phi(x^*, \eta, t^*)}{\partial \eta} \frac{\partial \eta(x^*, y^*, t^*)}{\partial t^*}, \qquad [42]$$

where the additional terms involving the derivative of η with respect to x^*, y^* and t^* are obtained from [41] to yield

$$\frac{\partial \eta}{\partial t^*} = -\frac{\dfrac{\partial y_b^*}{\partial t^*} + \eta\left(\dfrac{\partial y_t^*}{\partial t^*} - \dfrac{\partial y_b^*}{\partial t^*}\right)}{y_t^* - y_b^*},$$

$$\frac{\partial \eta}{\partial x^*} = -\frac{\dfrac{\partial y_b^*}{\partial x^*} + \eta\left(\dfrac{\partial y_t^*}{\partial x^*} - \dfrac{\partial y_b^*}{\partial x^*}\right)}{y_t^* - y_b^*}$$

and

$$\frac{\partial \eta}{\partial y^*} = \frac{1}{y_t^* - y_b^*}. \qquad [43]$$

In order to determine the concentration profiles in the resuspended layer we shall invoke a pseudo-steady-state assumption. We assume that the rate of deposition and erosion is sufficiently slow that the concentration profiles within the layer as seen by an observer in the coordinate system (x^*, η, t^*) fixed to the layer are steady. This is equivalent to assuming that the profile acquires some steady shape which simply moves with the eroding bed. As a consequence, in the (x^*, η, t^*) coordinate system, $\partial \phi / \partial t^* = 0$. This approximation will be reasonable provided that the turbulent eddies persist for a sufficiently long period of time for the profiles in the layer to assume a steady form. In using [21]–[23] to represent the velocity profile, we have assumed that the sediment layer is flat. Obviously, this initial profile will evolve as the bed erodes. However, the approximation of a flat surface will be reasonable provided that the magnitude of the deformation is small with respect to the horizontal width of the eddies. The psuedo-steady-state assumption also implies that the top and bottom surfaces are moving at the same velocity (which will be a function of x^*) and hence the bottom velocity $\partial y_b^* / \partial t^*$, defined as $\dot{y}_b^*$, is equal to the top velocity $\partial y_t^* / \partial t^*$, defined as $\dot{y}_t^*$. The thickness of the resuspended layer is a function of x^* only and we account for this by defining another variable y_d^* equal to $y_t^* - y_b^*$. The mass-balance equation [39] is transformed by

[41]–[43] to yield the following equation for the steady motion of a resuspended layer:

$$-\frac{\dot{y}_b^*}{y_d^*}\frac{\partial\phi}{\partial\eta} = -y_d^* S\left[\left(\sin x^* \int_{-\infty}^{\eta}\frac{1}{\mu_r}\,d\eta\left[\frac{\partial\phi}{\partial x^*}-\frac{\eta}{y_d^*}\frac{\partial y_d^*}{\partial x^*}\frac{\partial\phi}{\partial\eta}\right]\right)-\left(\cos x^*\int_{-\infty}^{\eta}\int_{-\infty}^{\eta'}\frac{1}{\mu_r}\,d\eta''\,d\eta'\right.\right.$$
$$\left.\left.-\sin x^*\int_{-\infty}^{\eta'}\int_{-\infty}^{\eta'}\frac{1}{\mu_r^2}\frac{d\mu_r}{d\phi}\left[\frac{\partial\phi}{\partial x^*}-\frac{\eta}{y_d^*}\frac{\partial y_d^*}{\partial x^*}\frac{\partial\phi}{\partial\eta}\right]d\eta''\,d\eta'\right)\frac{\partial\phi}{\partial\eta}\right]$$
$$+\frac{\hat{D}}{\mu_r y_d^{*2}}\frac{\partial^2\phi}{\partial\eta^2}+\frac{d}{d\phi}\left(\frac{\hat{D}}{\mu_r}\right)\left(\frac{\partial\phi}{y_d^*\partial\eta}\right)^2+\frac{f+\phi\dfrac{df}{d\phi}}{y_d^*}\frac{\partial\phi}{\partial\eta}. \qquad [44]$$

The boundaries of the resuspended layer will move at velocities determined by the local flux conditions near the fully packed layer at the bottom and the clear fluid interface at the top. Since the concentration gradients as $\phi\to\phi_m$ at the bottom and as $\phi\to 0$ at the top grow without bound, we may approximate the sharp interfaces as a discontinuity in the concentration and flux profiles as follows. We choose two small numbers ϵ_t and ϵ_b and apply [44] as the valid mass-balance relation in the concentration range $(\phi_m-\epsilon_b\leqslant\phi\leqslant\epsilon_t)$ within the resuspended layer, as shown in figure 8. The approximation of a sharp interface as a jump in the concentration and flux profiles at the interface is used to obtain the velocity with which the interface moves in response to the local concentration and flux discontinuity. Let AB be a small section of the interface between any two regions labelled L and U across which we have a discontinuity in the concentration and flux. The velocity V with which the interface moves is obtained from a mass balance around the dotted envelope shown in figure 8. We note that the interface moves as a result of $(\mathbf{N}_L-\mathbf{N}_U)\cdot\hat{\eta}$ (the component of net flux jump in the direction normal to the interface) and can be expressed as

$$\mathbf{V}=\frac{[(\mathbf{N}_L-\mathbf{N}_U)\cdot\hat{\eta}]\hat{\eta}}{\phi_L-\phi_U}, \qquad [45]$$

where $\mathbf{N}_L$, $\mathbf{N}_U$ and ϕ_L, ϕ_U are the flux vectors and concentrations in the two regions L and U, respectively, and $\hat{\eta}$ is the unit vector in the direction normal to AB.

Applying [45] to the bottom boundary and noting that $\mathbf{N}_L=0$ in the fully packed layer and $\mathbf{N}_U=N_y$ for a flat surface, the following equation for the movement of the bottom boundary is obtained:

$$\frac{\partial y_b}{\partial t}=-\frac{N_y}{\phi_m-\phi}=\frac{1}{\phi_m-\phi}\left[\frac{\hat{D}\tau a^2}{\mu_0\mu_r}\frac{\partial\phi}{\partial y}+u_s f\phi\right]\Bigg|_{\phi=\phi_m-\epsilon_b}. \qquad [46]$$

Equation [45] is rendered dimensionless by the previously obtained scaling factors for length and time and then y^* is transformed to η to obtain

$$\dot{y}_b^*=\frac{1}{\phi_m-\phi}\left[\frac{\hat{D}}{\mu_r y_d^*}\frac{\partial\phi}{\partial\eta}+f\phi\right]\Bigg|_{\phi=\phi_m-\epsilon_b}. \qquad [47]$$

We similarly apply [45] by substituting for the flux $\mathbf{N}_L$ in terms of N_x and N_y at an inclined interface to determine the dimensionless motion of the top boundary:

$$\dot{y}_t^*=-\frac{1}{\left(1+a_R^2\left[\dfrac{\partial y_d^*}{\partial x^*}\right]^2\right)}$$
$$\times\left\{Sy_d^*\frac{\partial y_d^*}{\partial x^*}\sin x^*\int_{-\infty}^{\eta}\frac{1}{\mu}\,d\eta'+Sy_d^{*2}\left(\cos x^*\int_{-\infty}^{\eta}\int_{-\infty}^{\eta'}\frac{1}{\mu_r}\,d\eta''\,d\eta'\right.\right.$$
$$\left.\left.-\sin x^*\int_{-\infty}^{\eta}\int_{-\infty}^{\eta'}\frac{1}{\mu_r^2}\frac{d\mu_r}{d\phi}\frac{\partial\phi}{\partial x^*}\,d\eta''\,d\eta'\right)+\frac{1}{\phi-\phi_\infty}\left\{\frac{\hat{D}}{\mu_r y_d^*}\frac{\partial\phi}{\partial\eta}+[f(\phi)\phi-f(\phi_\infty)\phi_\infty]\right\}\right., \qquad [48]$$

where $a_R=9\pi\psi a/\lambda$ (the ratio of the two length scales L_s and $\lambda/2\pi$) and ϕ_∞ is the concentration of particles in the bulk of the fluid far away from the wall.

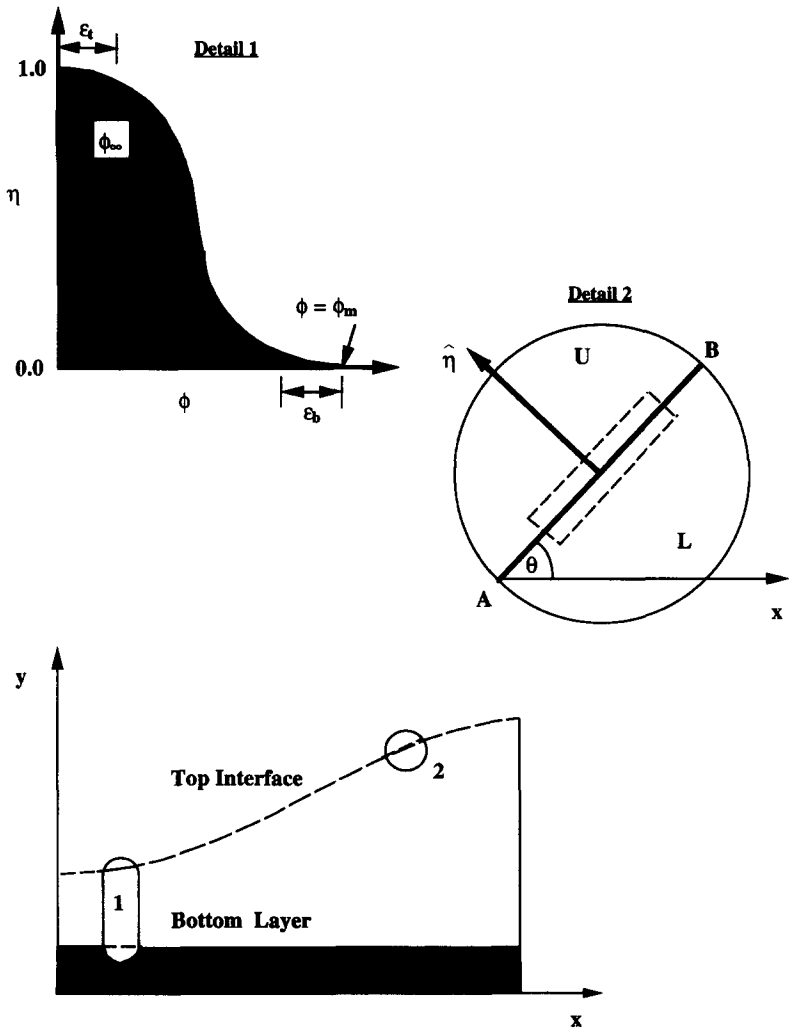

Figure 8. The slope of the concentration profiles, as shown in detail 1, becomes unbounded due to the shear-induced diffusivity becoming zero at the bottom settled layer and the top edge of the resuspended layer. The convection–diffusion equations are applied in the region $\phi_\infty - \epsilon_t < \phi < \phi_m - \epsilon_b$. In detail 2, the top (between ϕ_∞ and $\phi_\infty - \epsilon_t$) and bottom (between $\phi_m - \epsilon_b$ and ϕ_m) regions are shown modeled as discontinuities in concentration and fluxes. A material balance around the dotted envelope will yield the velocity at which the interfaces move.

The model derived above for the motion of the upper and lower interfaces essentially assumes that there is no resistance for the bed to unpack between ϕ_{max} and $\phi_{max} - \epsilon_b$ or for the transition of the upper interface between $\phi = \epsilon_t$ and $\phi = 0$. While this is reasonable for the upper interface, it is more questionable for the settled bed. If the bed consists of cohesive sediments (such as clay particles, for example) then there may be considerable resistance to "breaking loose" the sediment from the packed layer. Without detailed knowledge of the cohesive forces present, however (which may vary with the type of sediment), the assumption of no resistance (e.g. a noncohesive sediment) is the chosen way to close the model. For our calculations, ϵ_b and ϵ_t were chosen to be 0.02, however, the concentration profiles were insensitive to changing these parameters by a factor of 2.

So far, we have assumed that we have a clear fluid at the top of the resuspended particle layer in order to consider the more complex problem of two moving interfaces. However, in general, we may have a nonzero concentration of particles on the top of the resuspended layer and this leads us to consider the modified problem when $\phi \to \phi_\infty$ as $y \to \infty$. We may note that as long as $\phi_\infty \neq 0$, the slope of the concentration profile $\partial\phi/\partial y^*$ is bounded at the upper interface. However, for small values of ϕ_∞ we have a small region at some y^* where we expect a large but bounded concentration

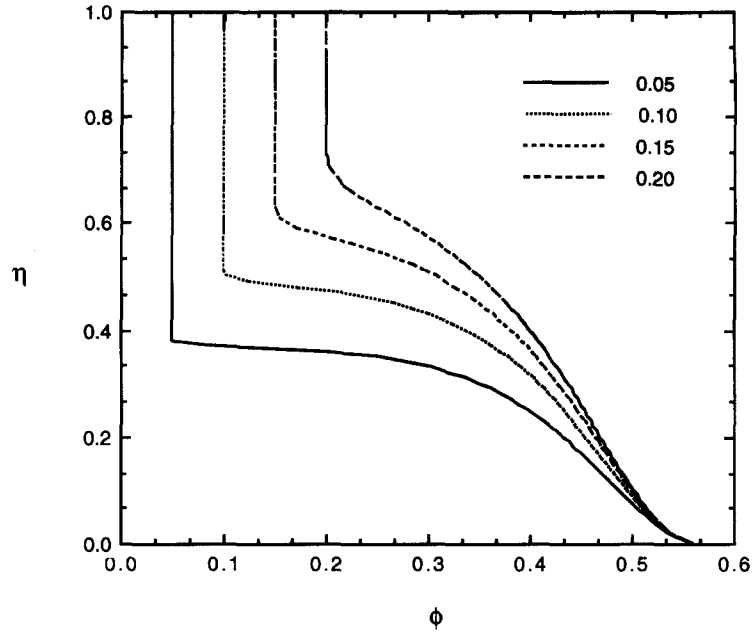

Figure 9. Plot of the initial concentration profile $\phi(x^* = 0, \eta)$ for $\phi_\infty = 0.2$ to 0.05 in the case of the nonlinear turbulent resuspension problem. Note the development of a sharp interface at the top for small values of ϕ_∞.

gradient $\partial\phi/\partial y^*$, due to a small but nonzero ϕ at the top, after which the concentration profile approaches a flat region where essentially $\phi \approx \phi_\infty$. This is due to the vanishingly small diffusion coefficient in this region of large concentration gradients [$D \to O(\phi^2)$ for small values of ϕ]. In figure 9 we have plotted the initial concentration profiles at $x^* = 0$ for various values of ϕ_∞. The development of a sharp interface is clearly evident when ϕ_∞ is less than about 0.1. Also, when $\phi_\infty \approx 0.05$ or less, the region of large concentration gradient is almost indistinguishable from a discontinuity. The region of large concentration gradient disappears when ϕ_∞ is approximately greater than 0.15 and we observe a smooth transition of the concentration profile into the bulk of the suspension. As a result, we can no longer define an upper boundary for the resuspended layer.

In order to solve the nonlinear problem for all ranges of bulk concentrations, we use two approaches. For small values of ϕ_∞, we let y_d^* represent the true thickness of the resuspended layer when a region of large gradient in concentration exists. Equation [47] then gives the velocity with which the top interface moves. In the second case, applicable when ϕ_∞ is large, y_d^* no longer represents the thickness of the resuspended layer. Instead, it is an arbitrarily large number, which does not depend on x^*, chosen to impose the boundary condition far from the wall $\phi = \phi_\infty$ in much the same manner as a large value of L_n was chosen for the upper boundary in the linearized problem. We also expect that in the intermediate range of concentrations we may solve the problem by either assumption and the two results should be comparable.

We impose the boundary conditions $\phi = \phi_m - \epsilon_b$ at $\eta = 0$ and $\phi = \phi_\infty - \epsilon_t$ at $\eta = 1$. The initial condition in the downwelling region is obtained by substituting $x^* = 0$ in the mass-conservation equation [43] and solving the nonlinear equation which is now a function of η alone. Equation [47] gives $\dot{y}_b^*$, the velocity with which the bottom moves. This is the variable introduced in [44] as a result of our earlier transformation of variables. In order to satisfy the pseudo-steady-state assumption, we must impose the additional restriction that the top and bottom boundaries move at the same velocity. This is readily achieved by adjusting the thickness of the resuspended layer y_d^*. The initial concentration profile is solved by a shooting technique starting with an initial guess for the variables y_d^* and $\partial\phi/\partial\eta$ at $\eta = 0$, which are iteratively improved by applying the Newton–Raphson method to satisfy the boundary condition at $\eta = 1$ and the requirement that

the bottom and top boundaries move at the same velocity. As we have already demonstrated in the case of the linear problem in the earlier section, we make use of the condition that the concentration distribution $\phi(x^*, \eta)$ is independent of x^* as $x^* \to 0$.

The complete concentration profile $\phi(x^*, \eta)$ is solved from the initial conditions in the downflow region $x^* = 0$ up to the upflow region $x^* = \pi$ by discretizing the concentration profile on a uniform grid in η space. The concentration vector representing the concentration values at the various grid positions is augmented by the additional variable y_d^* and integrated from $x^* = 0$ as an implicit set of differential and algebraic equations (DAEs) using the DASSL Fortran code for solving DAE models. We obtain the integrated average flux at the bottom in terms of the net integrated erosion/deposition of the bottom packed layer for various values of ϕ_∞ as a function of the parameter $S^{1/3}$, as shown in figure 10. When S is small (corresponding to the case of weak convection in the resuspended layer), we have a net deposition of particles on the bottom bed as a result of downward settling of particles from infinity impressed upon the resuspended particle layer. The net deposition due to this downward settling of particles from infinity remains almost unchanged by increasing values of S up to $S^{1/3} \approx 1$. At higher values of S, we observe a small transition region characterized by rapidly decreasing bed deposition rates. This reduction in bed deposition rates is due to an increasing fraction of the downward settling of particles which are able to escape the resuspended layer with increasing strength of the turbulent eddies. With increasing S and finite ϕ_∞, the erosion of the bed eventually overcomes the sedimentation from outside the layer and the net deposition rate becomes negative. For large values of S, the change in the net bed deposition rate with $S^{1/3}$ asymptotically approaches a straight line. The slope of this line for large values of S is identical for various values of ϕ_∞. Hence, the incremental flux as a result of any given change in the parameter S becomes proportional to the change in $S^{1/3}$. This scaling for the net deposition rate, valid for large values of S, is similar to the linearized problem examined in the earlier section. As before, this limiting net deposition rate (which is analogous to the dimensionless mass flux) is independent of gravity driven sedimentation and is the result of a balance between diffusive and convective terms.

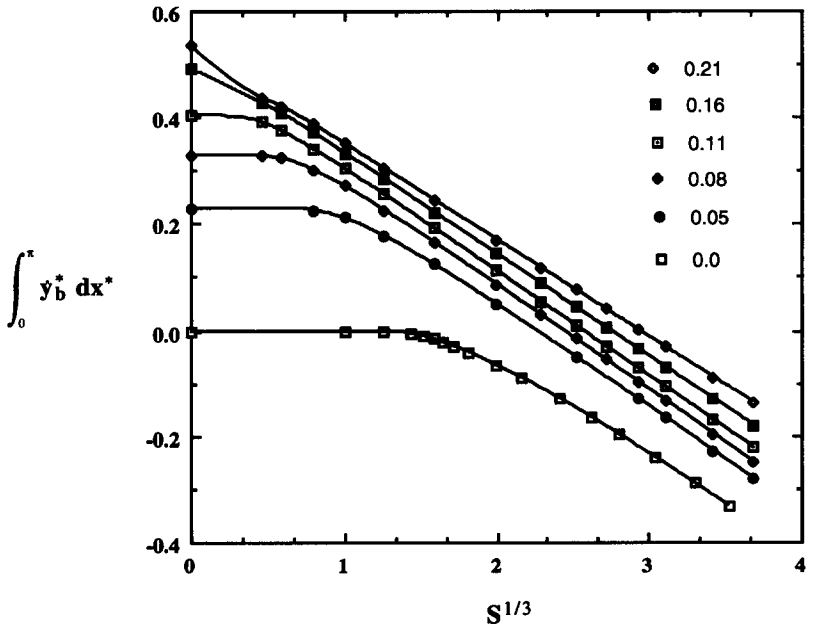

Figure 10. Plot of the dimensionless net motion of the bottom layer of particles when $\phi_\infty = 0$ to 0.21 as a function of the dimensionless parameter $S^{1/3}$. Note that for large S, the dimensionless net motion asymptotes to a straight line.

6. COMPARISON WITH EXPERIMENTAL RESULTS

We are not aware of any experiments which determine the point at which particles are first ejected from the viscous sublayer into the turbulent core. Essentially, this would correspond to the point where significant bed erosion occurs since the thin viscous sublayer has a very limited capacity for sediment transport. We can, however, compare our theoretical prediction to the Shields criterion for first motion of a settled bed and to the minimum transport friction velocity for the complete resuspension of a settled layer, which is done in figure 11.

The Shields criterion for the onset of particle motion reported by Yalin & Karahan (1979) (valid when the particle Reynolds number is approximately less than unity) is

$$\psi_{cr} = \frac{0.2}{(\mathrm{Re}_p^+)^{0.3}}. \qquad [49]$$

This correlation is tested with experimental data up to the lowest reported particle Reynolds number of about 0.04. The correlation suggests the critical Shields parameter becomes infinite as $\mathrm{Re}_p^+ \to 0$, thus requiring an infinite shear stress to move the bed at zero Reynolds number. At sufficiently low particle Reynolds numbers, however, we expect the first motion to occur when viscous forces (which scale with $\tau_0 a^2$) balance gravitational forces; e.g. when the Shields parameter equals some constant. Thus, it is physically more realistic to expect the critical Shields parameter to asymptotically approach this constant value as $\mathrm{Re}_p^+ \to 0$. In the viscous resuspension experiments, Leighton & Acrivos (1986) observed the first motion of a settled bed at low Reynolds number (≈ 0.02) to occur at $\psi = 0.5$. This value is quite close to the critical Shields parameter reported by Yalin & Karahan (1979) at the lowest particle Reynolds number reported in that study. The Shields criterion given by [49] can be expressed as

$$\frac{u_s}{u_*} \leqslant 0.55(\mathrm{Re}_p^+)^{1.3}. \qquad [50]$$

Equation [50] is shown as the dashed line (top left) in figure 11.

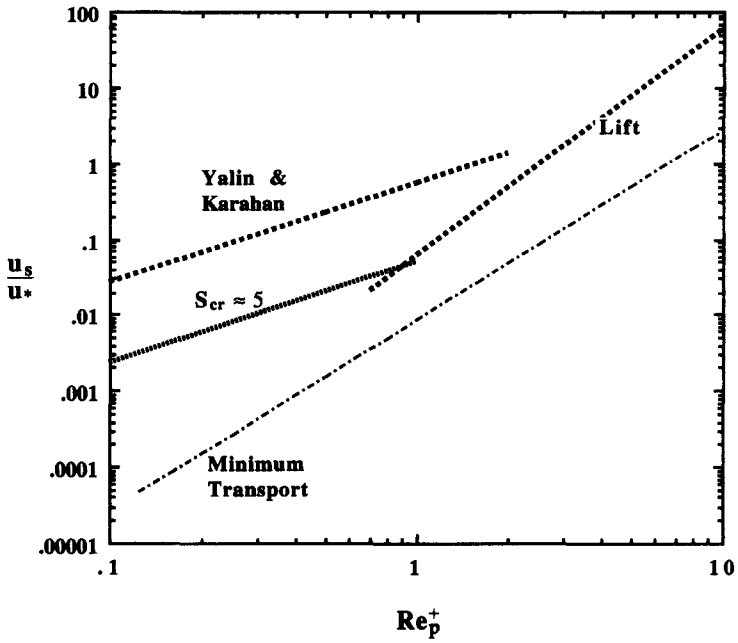

Figure 11. Comparison of the results of viscous resuspension with Shields criteria for the first motion of the settled bed and the minimum transport velocity. The inertial lift mechanism becomes dominant when $\mathrm{Re}_p^+ > \sim 1$.

The minimum transport velocity is the empirically determined friction velocity at which the particles first begin to settle out at the walls of a pipe and form a sliding sediment layer. The limiting value of this minimum transport velocity for suspensions at low concentrations was found by Thomas (1961) to be

$$\frac{u_s}{u_*} \geqslant 0.0084\,(\mathrm{Re}_p^+)^{2.5}, \qquad [51]$$

which is also plotted (bottom line) in figure 11. Note that a sliding sediment layer will form for all conditions above and to the left of this line.

The leftmost line in the middle of figure 11 is the point where we predict particles will be first ejected from the viscous sublayer into the turbulent core. This corresponds to the case when S is greater than the critical value $S_{cr} \approx 5$, which is equivalent to

$$\frac{u_s}{u_*} \leqslant 0.05\,(\mathrm{Re}_p^+)^{4/3}. \qquad [52]$$

Balancing the inertial lift experienced by a particle sitting on a plane in the presence of uniform shear flow (Leighton & Acrivos 1985) with the net gravitational force acting on the particle, we obtain the rightmost line shown in the middle of the figure 11 from the inequality

$$\frac{u_s}{u_*} \leqslant 0.061\,(\mathrm{Re}_p^+)^3. \qquad [53]$$

The two lines in the middle intersect at $\mathrm{Re}_p^+ \approx 0.9$. As expected, viscous resuspension effects will dominate when $\mathrm{Re}_p^+ < \sim 1$. This condition can be expressed in terms of the fluid properties and particle size:

$$\frac{a^3\,\Delta\rho g \rho}{\mu^2} < 0.091. \qquad [54]$$

For the case of turbulent resuspension of river bed sediments, for example, from [54] we estimate that viscous effects will be important when $d_p < 42\,\mu$m. We have assumed the properties of water with $\rho = 1.0$ g/cm^3, $\Delta\rho = 1.0$ g/cm^3 and $\mu = 1$ cP. This is considerably smaller than the characteristic diameter of river sediment, thus it is unlikely that shear-induced migration plays an important role for the turbulent resuspension of such sediments. For larger viscosities and a smaller density difference, the transition occurs for much larger particles. For a suspension of acrylic particles in ethylene glycol, for example ($\rho = 1.11$ g/cm^3, $\Delta\rho = 0.07$ g/cm^3 and $\mu = 20$ cP), the critical diameter increases to $d_p = 720\,\mu$m. There may be other systems (a coal–oil slurry, for example, or drilling muds) where the characteristic particle size is small enough or the fluid viscosity is high enough that viscous effects will dominate resuspension.

Our prediction, with no adjustable parameters, as shown in figure 11, falls midway between the first motion criterion and the complete resuspension condition for small particle Reynolds numbers, as would be expected if the theory were valid. This qualitative agreement between the theory and the experiment provides strong evidence that the resuspension of particles at low Reynolds numbers in the near-wall region is influenced by the shear-induced migration processes described in the model given here. A more detailed description of turbulent resuspension in this parameter regime requires a more sophisticated model of near-wall turbulence and the inclusion of transient phenomena. Such analysis is left to future work.

Acknowledgements—The authors would like to acknowledge helpful conversations with Dr M. J. McCready (Chemical Engineering Department, University of Notre Dame) and Dr David McTigue (Sandia National Laboratory). This work was supported, in part, by the National Science Foundation and by the Petroleum Research Fund of the American Chemical Society.

REFERENCES

CAMPBELL, J. A. & HANRATTY, T. J. 1983 Mechanism of turbulent mass transfer at a solid boundary. *AIChE Jl* **29,** 221–229.

CHAPMAN, B. K. & LEIGHTON, D. T. 1991 Dynamic viscous resuspension. *Int. J. Multiphase Flow* **17,** 469–483.

FINNICUM, D. S. & HANRATTY, T. J. 1985 Turbulent normal velocity fluctuations close to a wall. *Phys. Fluids* **28,** 1654–1658.

GADALA-MARIA, F. A. 1979 The rheology of concentrated suspensions. Ph.D. Thesis, Stanford Univ., CA.

HUNT, J. N. 1954 The turbulent transport of suspended sediment in open channels. *Proc. R. Soc. Lond.* **A224,** 322–335.

LEIGHTON, D. T. & ACRIVOS, A. 1985 The lift on a small sphere touching a plane in the presence of a simple shear flow. *Z. Angew. Math. Phys.* **36,** 174–178.

LEIGHTON, D. T. & ACRIVOS, A. 1986 Viscous resuspension. *Chem. Engng Sci.* **41,** 1377–1384.

LEIGHTON, D. T. & ACRIVOS, A. 1987 Shear-induced migration of particles in concentrated suspensions. *J. Fluid Mech.* **181,** 415–439.

MANTZ, P. 1977 Incipient transport of fine grains and flakes by fluids—extended Shields diagram. *ASCE Jl Hydraul.* **103,** 601–656.

MCTIGUE, D. F. 1983 Mixture theory for turbulent diffusion of heavy particles. In *Theory of Dispersed Multiphase Flow* (Edited by MEYER, R. E.). Academic Press, New York.

SAFFMAN, P. G. 1965 The lift on a small sphere in a slow shear flow. *J. Fluid Mech.* **22,** 385–400.

THOMAS, D. G. 1961 Transport characteristics of suspensions: II. Minimum transport velocity for flocculated suspensions in horizontal pipes. *AIChE Jl* **7,** 423–430.

YALIN, M. S. 1972 *Mechanics of Sediment Transport.* Pergamon Press, Oxford.

YALIN, M. S. & KARAHAN, E. 1979 Inception of sediment transport. *ASCE Jl Hydraul.* **105,** 1433–1443.

YUNG, B. P. K., MERRY, H. & BOTT, T. R. 1989 The role of turbulent bursts in particle re-entrainment in aqueous systems. *Chem. Engng Sci.* **44,** 873–882.